AIP | The Journal of Chemical Physics

Excited state dynamics of acrylonitrile: Substituent effects at conical intersections interrogated via time-resolved photoelectron spectroscopy and ab initio simulation

Ryan J. MacDonell, Oliver Schalk, Ting Geng, Richard D. Thomas, Raimund Feifel, Tony Hansson, and Michael S. Schuurman

Citation: The Journal of Chemical Physics **145**, 114306 (2016); doi: 10.1063/1.4962170
View online: http://dx.doi.org/10.1063/1.4962170
View Table of Contents: http://scitation.aip.org/content/aip/journal/jcp/145/11?ver=pdfcov
Published by the AIP Publishing

Excited state dynamics of acrylonitrile: Substituent effects at conical intersections interrogated via time-resolved photoelectron spectroscopy and *ab initio* simulation

Ryan J. MacDonell,[1] Oliver Schalk,[2,a)] Ting Geng,[2] Richard D. Thomas,[2] Raimund Feifel,[3] Tony Hansson,[2] and Michael S. Schuurman[1,4,b)]

[1]*Department of Chemistry and Biomolecular Sciences, University of Ottawa, D'Iorio Hall, 10 Marie Curie, Ottawa, Ontario K1N 6N5, Canada*
[2]*Department of Physics, AlbaNova University Center, Stockholm University, Roslagstullsbacken 21, 106 91 Stockholm, Sweden*
[3]*Department of Physics, University of Gothenburg, Origovägen 6B, 412 96 Gothenburg, Sweden*
[4]*National Research Council of Canada, 100 Sussex Drive, Ottawa, Ontario K1A 0R6, Canada*

(Received 19 May 2016; accepted 22 August 2016; published online 20 September 2016)

We report a joint experimental and theoretical study on the photoinitiated ultrafast dynamics of acrylonitrile (AN) and two methylated analogs: crotonitrile (CrN) and methacrylonitrile (MeAN). Time-resolved photoelectron spectroscopy (TRPES) and *ab initio* simulation are employed to discern the conical intersection mediated vibronic dynamics leading to relaxation to the ground electronic state. Each molecule is pumped with a femtosecond pulse at 200 nm and the ensuing wavepackets are probed by means of one and two photon ionization at 267 nm. The predominant vibrational motions involved in the de-excitation process, determined by *ab initio* trajectory simulations, are an initial twisting about the C═C axis followed by pyramidalization at a carbon atom. The decay of the time-resolved photoelectron signal for each molecule is characterized by exponential decay lifetimes for the passage back to the ground state of 60 ± 10, 86 ± 11, and 97 ± 9 fs for AN, CrN, and MeAN, respectively. As these results show, the excited state dynamics are sensitive to the choice of methylation site and the explanation for the observed trend may be found in the trajectory simulations. Specifically, since the pyramidalization motion leading to the conical intersection with the ground state is accompanied by the development of a partial negative charge at the central atom of the pyramidal group, the electron donation of the cyano group ensures that this occurs exclusively at the medial carbon atom. In this way, the donated electron density from the cyano group "directs" the wavepacket to a particular region of the intersection seam. The excellent agreement between the experimental and simulated TRPES spectra, the latter determined by employing trajectory simulations, demonstrates that this mechanistic picture is consistent with the spectroscopic results. [http://dx.doi.org/10.1063/1.4962170]

I. INTRODUCTION

Interest in the photochemistry of α,β-enenitriles, here exemplified by acrylonitrile (AN, 2-propenenitrile), crotonitrile (CrN, 2-butenenitrile), and methacrylonitrile (MeAN, 2-methyl-2-propenenitrile) illustrated in Figure 1, stems in part from their unusual photodissociation dynamics. Whereas most nitriles eliminate radical CN following UV excitation,[1–3] acrylonitrile is observed to release molecular HCN and H_2. These photodissociation dynamics were first studied by Gandini and Hackett using a 213.9 nm excitation wavelength to prepare the $\tilde{A}^1A'$ state. They observed the aforementioned molecular dissociation products, as well as significant hydrogen/deuterium scrambling in the HCN and H_2 products when the 2-carbon was deuterated, which they ascribed to an excited state H/D scrambling process.[4] The observations of HCN and H_2 dissociation products were consistent with more recent theoretical determinations of the expected photoproducts following 193 nm photoexcitation.[5] However, CN elimination was also observed for AN, CrN, and MeAN following excitation at 193 nm.[6,7] *Ab initio* calculations show that MeAN, unlike AN and CrN, may overcome the barrier to CN and H migration before dissociation.[7]

The conjugated π system of α,β-enenitriles gives rise to several low-lying electronic states, resulting in a complex electronic structure that has been the subject of numerous spectroscopic characterization studies.[4,8–10] In the first reported absorption spectrum of AN, the two overlapping absorption bands were observed to lie between 159 and 213 nm (5.8–7.8 eV)[8] and were assigned to $n \rightarrow \pi^*$ and $\pi \rightarrow \pi^*$ transitions.[4,8] Using electron energy loss spectroscopy and high resolution photoabsorption spectroscopy, these peaks were later reassigned to the $\pi_2(C{=}C{-}C{\equiv}N) \rightarrow \pi_1^*(C{=}C{-}C{\equiv}N)$ transition ($\tilde{A}^1A'$) and the $\pi_2(C{=}C{-}C{\equiv}N) \rightarrow \pi^*(C{\equiv}N)$ transition ($\tilde{B}^1A''$). An additional band in the range of 138–177 nm

a)Electronic mail: oliver.schalk@fysik.su.se
b)Electronic mail: michael.schuurman@nrc-cnrc.gc.ca

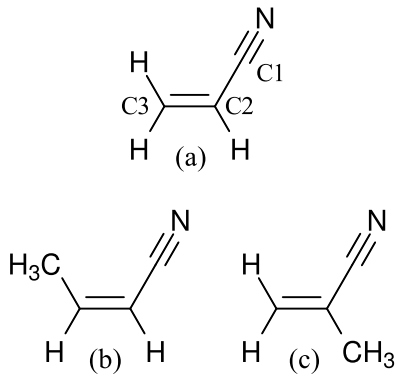

FIG. 1. Molecular structures of (a) acrylonitrile, (b) *cis*-crotonitrile, and (c) methacrylonitrile. Carbon atom labels are consistent for all three molecules.

(7.0–9.0 eV) was assigned to the $\tilde{C}^1A'$ (π_2(C═C—C≡N) → π_2^*(C═C—C≡N)) transition, while higher energy bands were attributed to a Rydberg series.[9,10] To date, high-resolution characterization of the electronic spectra has not been performed for CrN and MeAN, but low resolution UV-Vis spectra show similar broad overlapping bands in the 200–225 nm (5.5–6.2 eV) range.[7]

The potential energy surfaces of the ground state and low lying excited states of AN have been extensively studied to characterize and enumerate the dissociative pathways associated with excitation at 193 nm. Du *et al.*[5] optimized potential energy minima, transition states, and minimum energy conical intersections (MECIs) for singlet and triplet states in the Franck-Condon (FC) region. They found that minimum energy structures were not present for the first and second singlet excited states (S_1 and S_2, respectively) in the FC region. Instead, gradients on both surfaces direct the molecule to a conical intersection (CI) to the lower energy state. The S_2-S_1 MECI corresponds to the ground state equilibrium geometry with 90° torsion about the C═C bond, while the MECI between S_1 and the ground state involves both the C═C torsion as well as a C═C—C bend. Thus, after excitation to S_2, the molecule was predicted to decay through both CIs to the ground state. The molecule in the ground state would then have sufficient internal energy to dissociate.[5]

Acrylonitrile has also been studied as a model system for near edge x-ray absorption fine structure spectroscopy (NEXAFS).[11,12] The two low-lying π^* orbitals give rise to high intensity peaks corresponding to excitation into these anti-bonding orbitals from the N 1s orbital. Assignment of the vibrational structure was achieved using density functional theory (DFT) to determine the Franck-Condon transition amplitudes, providing good agreement between theoretical and experimental spectra.[11,12] A further study with a higher energy probe found a closely spaced doublet corresponding to N 1s excitation to a diffuse Rydberg type orbital and an additional $\pi^*(A'')$ orbital. Excitation to the Rydberg-type orbital led to out-of-plane motion of CCN and CH_2 groups, whereas excitation to the π^* orbital caused in-plane CCC and CCN bending.[12]

In order to more definitively address the mechanism of ultrafast relaxation in α,β-enenitriles, this study uses time-resolved photoelectron spectroscopy (TRPES) together with *ab initio* molecular dynamics simulations to discern the excited state dynamics of AN. The time scales associated with electronic de-excitation are probed directly via experiment, while the atomic motions associated with the molecular dynamics are obtained using on-the-fly *ab initio* calculations.[13–15] Using methyl substitution, the relative importance of different internal motions can be discerned from excited state decay time scales by experimental and theoretical means. This technique has been previously used in, for example, time-resolved studies of ethylene,[16] 1,3-cyclopentadiene,[17,18] and α,β-enones.[19,20] Here, we employ a pump wavelength of 200 nm for all molecules which prepared molecules in both the first and second excited states, $\tilde{A}^1A'$ and $\tilde{B}^1A''$, and perform *ab initio* molecular dynamics simulations that are then employed to generate a theoretical TRPES signal for direct comparison to experimental results.

II. METHODS

A. Experimental methods

AN, MeAN, and CrN were purchased from Sigma-Aldrich with stated purities of 99% and were used without further purification. CrN was delivered and used as a mixture of *cis*- and *trans*-isomers. However, within the present experimental conditions, we expect the *cis*-isomer to be predominant (see below). Absorption spectra were taken in a 1 cm quartz cuvette (Hellma) at saturated vapor pressure using a Cary 5e photospectrometer (Varian). The magnetic bottle electron spectrometer setup used in the present study for time-resolved measurements was described before.[21,22] Briefly, it consists of a 5.6-m long flight tube with an energy ($E/\Delta E$) resolution of better than 100, which implies that the resolution for slow photoelectrons is limited by the spectral resolution of the laser pulses. Femtosecond laser pulses were obtained from a Ti:sapphire regenerative amplifier (Coherent Legend USP-HE) with an output energy of 4 mJ pulse^{-1} at a repetition rate of 1 kHz. Pump and probe pulses at 200 and 267 nm were generated by frequency doubling and consecutive mixing with the fundamental laser beam in β-barium borate crystals. In the experiments, the laser beams were attenuated to 100 nJ for the 200 nm pump and 3 μJ for the 267 nm probe pulses. They were focused weakly into the interaction region by a concave spherical aluminum mirror ($f/150$ for the pump and $f/125$ for the probe pulse). The cross correlation between pump and probe pulses was measured in xenon and was 160 ± 15 fs for a [1 + 1′] experiment. The spectral bandwidth of both pump and the probe pulses was around 25 meV. The time delay between the two pulses was controlled by a motorized linear translation stage. At each delay, the measured pump-probe signal was corrected by subtracting the background signals due to the pump and probe laser pulses alone. Perpendicular to the incoming laser pulses, the sample was inserted in the interaction region of the magnetic bottle spectrometer by means of an effusive gas needle using the vapor pressure of the investigated liquids. Within the present experimental conditions, a *cis-trans* mixture of CrN is expected with ~62% of the molecules in the *cis*-configuration.

B. Computational methods

Excited state trajectory simulations were performed by employing *ab initio* potential energy surfaces determined on-the-fly and propagated using the *ab initio* multiple spawning (AIMS) method.[23–25] Here, the wavefunction is the product of electronic and nuclear functions as expressed by

$$\Psi(\mathbf{r},\mathbf{R},t) = \sum_{I=1}^{N_s}\sum_{j=1}^{N_I(t)} c_j^I(t)\psi_j^I(\mathbf{r};\mathbf{R}_j^I(t)) \times \chi_j^I(\mathbf{R};\mathbf{R}_j^I(t),\mathbf{P}_j^I(t),\gamma_j^I(t)), \quad (1)$$

where $\mathbf{r}$ and $\mathbf{R}$ represent electronic and nuclear coordinates, respectively. The wavefunction expansion includes the number of states N_s relevant to the dynamics with electronic wavefunctions $\psi^I(\mathbf{r};\mathbf{R})$. The nuclear component of the trajectory basis function, χ_j^I, is expanded as a direct product of frozen Gaussian basis functions with a time-dependent position $\mathbf{R}_j^I(t)$, momentum $\mathbf{P}_j^I(t)$, and phase $\gamma_j^I(t)$, which evolve according to classical equations of motion. When trajectories enter a region with nonadiabatic coupling beyond a given threshold, they may spawn new basis functions on the coupled state. As a result, the number of basis functions on electronic state I, $N_I(t)$, is time-dependent. The complex amplitudes $c_j^I(t)$ of each trajectory are determined variationally at each time step according to the time-dependent Schrödinger equation.

The initial geometries and momenta of each molecule were sampled from the $v = 0$ vibrational Wigner distribution with the constraint that the excitation energy at a given point was within the pump pulse energy ± twice the laser bandwidth. In the FC region, the first and second excited states (S_1 and S_2, both $\pi\pi^*$ states) were nearly degenerate and had transition dipole moments on the same order of magnitude. For each initial condition, the probability of populating I is proportional to the oscillator strength scaled by the detuning from the central frequency of the pump envelope. More details can be found in the supplementary material. In order to correct for the theoretical and experimental energy differences between electronic states at the S_0 minimum, the S_1 energy was calculated using Davidson-corrected second-order multireference configuration interaction (MR-SOCI) with a 4s3p2d1f ANO basis set and using first-order multireference configuration interaction (MR-FOCI) with a 6-31G* basis. The difference in energies was then added to the pump energy of 6.20 eV (200 nm) during the selection of initial conditions. These energy shifts were 0.71, 0.74, and 0.69 eV for AN, CrN, and MeAN, respectively.

The trajectory simulations employed 31 (30) initial conditions for AN (MeAN), yielding a total of 559 (351) trajectories. To account for the mix of *cis* and *trans* CrN geometries, 29 initial conditions were *cis* geometry and 18 were *trans*. This gave rise to 505 and 285 trajectories, respectively.

At each time step, electronic wavefunctions necessary to propagate each basis function were calculated using the COLUMBUS electronic structure package.[26] The dynamics calculations were performed at the MR-FOCI/6-31G* level of theory.[27] The geometries of the S_0 minimum as well as S_2-S_1 and S_1-S_0 minimum energy conical intersections were optimized at this level of theory and checked with complete active space second-order perturbation theory (CASPT2) with a correlation-consistent triple zeta basis set (cc-pVTZ) calculations. Comparison of energy trends from MR-FOCI results with CASPT2 results was used to establish the accuracy of MR-FOCI/6-31G* for the dynamics simulation, as shown in Table S4 of the supplementary material. Although CASPT2 and MR-FOCI excitation energies differ by as much as 0.9 eV, the energy differences relevant to the dynamics (i.e., S_1 and S_2 at the S_0 minimum, the S_2-S_1 MECI, and the S_1-S_0 Tw-C2P MECI) are within 0.3 eV. Calculations for all three molecules employed an active space of six electrons in three π and three π^* orbitals for the complete active space self-consistent field (CASSCF) reference, with electronic character defined at the S_0 minimum geometry.

Direct comparison with the experimental spectra was undertaken by calculating the time-resolved photoelectron spectrum using the data produced from the AIMS trajectories. At each time step of each trajectory, MR-FOCI calculations were performed to determine the energy from the state of the trajectory to several doublet ion states. The total signal for ionization from electronic state I of the neutral to state α of the cation is given by the expression[15,28–30]

$$S(E,t) = \sum_{I=1}^{N_s^0}\sum_{j=1}^{N_I(t)} |c_j^I(t)|^2 \sum_{\alpha=1}^{N_s^+} W_{I\alpha}(\mathbf{R}_j^I(t)) \times \delta\left(E - [n\omega_2 - \Delta E_{I\alpha}(\mathbf{R}_j^I(t))]\right), \quad (2)$$

where ${N_s}^0$ and ${N_s}^+$ denote the number of neutral and cationic states, respectively, and $W_{I\alpha}$ is the probability of ionization from neutral state I to cationic state α. The energy portion of the spectrum includes the number of probe photons n (for one- or two-photon ionization), the probe pulse energy ω_2 and the ionization potential $\Delta E_{I\alpha}$. Thus, the energy for each trajectory j at time t is defined by the electron kinetic energy, $E = n\omega_2 - \Delta E_{I\alpha}$. Since the measurement we seek to simulate is angle-integrated, we chose to represent the ionization cross section arising from the matrix element above using the norm of the corresponding Dyson orbital, such that

$$W_{I\alpha}(\mathbf{R}_j^I(t)) \propto N\left|\langle\psi_j^\alpha(\mathbf{R}_j^I(t))|\psi_j^I(\mathbf{R}_j^I(t))\rangle\right|^2 = \left|\phi_{I\alpha}^D(\mathbf{R}_j^I(t))\right|^2, \quad (3)$$

for an N-electron system. In this way, we are limited to approximating the relative rates of ionization to different final cationic states. For 2-photon ionization, the transition corresponds to a set of intermediate neutral states and a transition probability of $W_{I\alpha} = 1$ was found to be a better approximation of the 2-photon signal. The final simulated spectrum was obtained by applying a Gaussian filter with full widths at half-maxima of 160 fs (140 fs in the 2-photon region) and 50 meV corresponding to the experimental time cross correlation and energy resolution, respectively.

III. RESULTS

A. UV-Vis absorption

The UV-Vis absorption spectra of AN, CrN, and MeAN are shown in Figure 2. These spectra are in agreement with

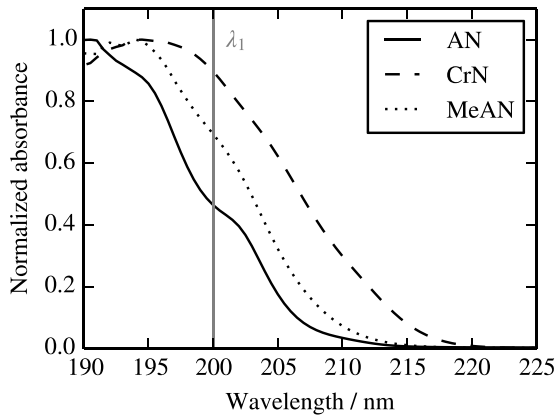

FIG. 2. Absorption spectra of acrylonitrile (AN), crotonitrile (CrN), and methacrylonitrile (MeAN). The pump wavelength (λ_1) of all three experiments is given by the vertical line.

more detailed spectra in the literature.[9,10] The broad absorption band of AN was found to originate at 211 nm (5.88 eV) and was assigned to a $\pi\pi^*$ state. Higher energy peaks were assigned to a vibrational progression.[10] The absorption spectra of MeAN and CrN are not readily assigned. Their corresponding absorption maxima are slightly red-shifted relative to AN and the broad band near 200 nm is similarly assigned to $\pi\pi^*$ excitation.

B. Potential energy surfaces

In the Franck-Condon region, the first two excited states both have $\pi\pi^*$ character. The optimization of minima on the pertinent potential energy surfaces, as well as minimum energy conical intersections between those surfaces, yields similar structural motifs for AN and its methylated analogs. Those that were found to be relevant to the dynamics after excitation to S_2 are shown in Figure 3, with geometries of each structure given in Figure S1 of the supplementary material. As noted by Du *et al.*[5] for AN, no potential energy minima

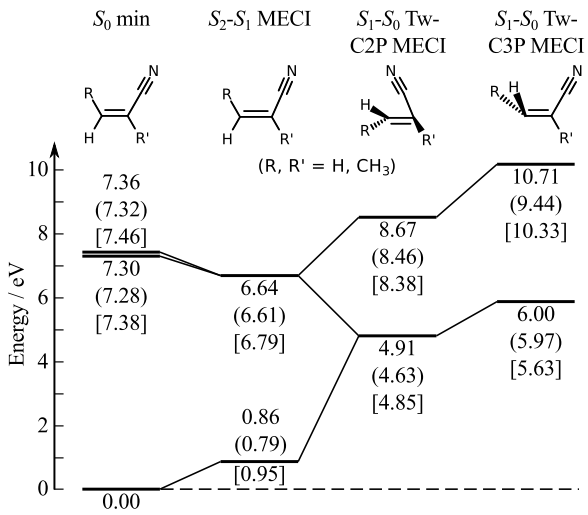

FIG. 3. Electronic energies of acrylonitrile (crotonitrile) [methacrylonitrile] at the critical points on the potential energy surface calculated at the MR-FOCI/6-31G* level of theory.

were found near the FC region on S_1 and S_2 for any of the molecules.

From Figure 3, it can be seen that the relative energies between the ground and low-lying excited states remain relatively unchanged upon methyl substitution for the regions of the potential energy surfaces relevant to this study. This is a desirable result in the sense that the effect of the methyl groups can be considered as primarily inertial or dynamical and does not appreciably change the contours of the electronic surfaces (in non-mass weighted coordinates). Each of the molecules have nearly degenerate first and second excited states in the Franck-Condon region. A S_2-S_1 MECI is found 0.7 eV below the S_2 energy at the FC point and is accessed through the elongation of the C=C bond. Likewise, each of the α,β-enenitriles has a S_1-S_0 MECI 1.7–2.0 eV lower in energy involving a C=C torsion, a C=C—C bend, and pyramidalization at carbon C2 relative to the ground state minimum. Additional MECIs corresponding to torsion and pyramidalization at C3 exist at a higher potential energy. These two MECI types will hereby be referred to as the Tw-C2P and Tw-C3P MECIs, respectively. The twist-pyramidalization S_1-S_0 MECI type is a common motif for CIs of molecules with a vinyl group.[16,19,30,31]

The CASPT2 values presented in Table S4 of the supplementary material are within 0.15 eV of the energies calculated by Du *et al.* Of note is the difference in optimized S_2-S_1 MECI geometries. Du *et al.* report a MECI involving a C=C torsion. In this work, two S_2-S_1 MECI geometries corresponding to the same conical intersection were optimized. Due to the strong coupling between S_2 and S_1 states in the Franck-Condon region, the geometry shown in Figure 3 was favoured. The same conical intersection is expected to mediate $S_2 \rightarrow S_1$ decay in the results of Du *et al.*[5]

C. Nonadiabatic dynamics simulation

Using the initial condition filtering procedure described in Section II B resulted in significant initial population on both S_1 and S_2 as a result of the nearby C=C stretch CI. The initial fraction of the wavepacket amplitude on S_2 varied between 0.5 and 0.9.

Figure 4 presents the adiabatic populations of the α,β-enenitriles as a function of time. For each of the three molecules, the initial population on S_2 decays rapidly to S_1 due to the easily accessible CI. The similarity in $S_2 \rightarrow S_1$ transitions is evinced by the time taken for the S_1 population to reach a maximum, which occurs around 60 fs for each of the molecules. There is a small increase in the S_2 decay time scale for MeAN relative to AN and CrN which may be related to an increase in the C=C bond length of the S_2-S_1 MECI as well as random errors in the data. The S_1 population then transitions to the ground state. The slow time scales relative to $S_2 \rightarrow S_1$ decay can be attributed to the large amplitude C=C torsion, C=C—C bend, and C2 pyramidalization. Interestingly, MeAN showed a much slower decay to the ground state despite the methyl group only undergoing a small out-of-plane motion to reach the Tw-C2P MECI. This can be seen quantitatively from the excited state lifetimes shown in Table I, where a single exponential fit to the total

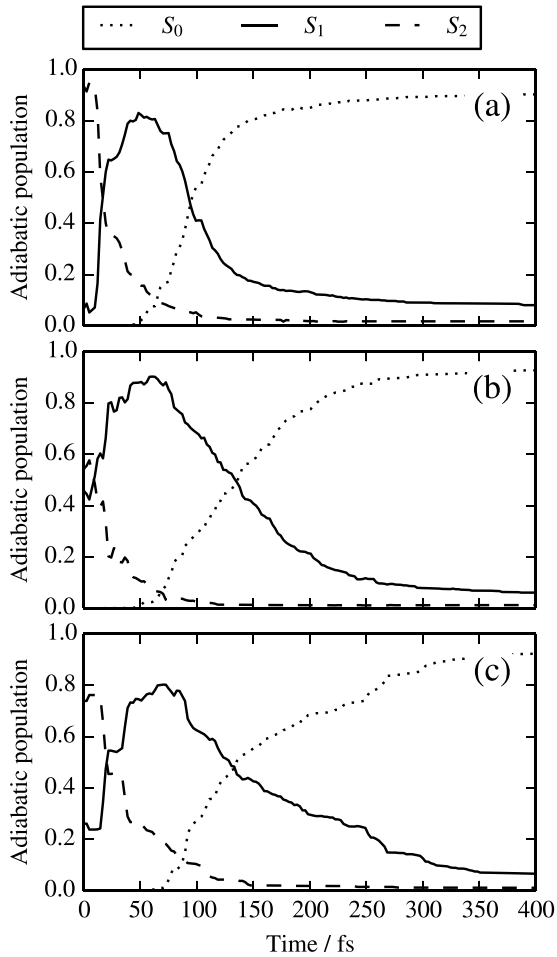

FIG. 4. Adiabatic populations *vs*. time for (a) AN, (b) CrN, and (c) MeAN. S_2 population rapidly transfers to the lower S_1 state, while the S_1 population must go through large amplitude motions to reach S_0.

excited state population ($S_1 + S_2$) yields increasing excited state lifetimes from AN to CrN to MeAN. The values given in Table I correspond to an exponential decay of the form $f(t) = \exp[-(t - t_{off})/\tau_{ex}]$ with a total excited state lifetime of $\tau_{tot} = t_{off} + \tau_{ex}$.

Despite both Tw-C2P and Tw-C3P being energetically accessible, ~95% of the population was found to travel through the S_2-S_1 CI followed by the Tw-C2P S_1-S_0 CI for AN and MeAN. CrN exhibited similar behaviour, with the exception that 15% of the *trans* population passed through the alternate CI. The C=C torsional angle was unimportant for the S_2-S_1 seam, with spawn geometry values varying from 0 to 90°. This can be seen in Figure 5, which plots the Monte Carlo integrated wavepacket density as a function of internal coordinate motion. Most of the initial S_2 wavepacket amplitude decays after a single C=C stretch. The remaining density stays on the S_2 state for multiple vibrational periods as the molecule simultaneously undergoes torsion about the C=C bond (see Figure 5(b)). The density plots corresponding to the wavepacket evolution for CrN and MeAN show the same trend; however, the decay to S_1 after a single C=C stretch is nearly quantitative. Also shown in Figure 5 is the S_1 population along the C=C—C bend and C=C torsion degrees of freedom, whereby most of the wavepacket transitions to the ground state following a single twist and bend.

TABLE I. Decay offsets, time constants, and total excited state lifetimes for single exponential fits to the total adiabatic excited state population. Standard deviations for least-squares fits are on the order of 1 fs for all values.

Molecule	t_{off}/fs	τ_{ex}/fs	τ_{tot}/fs
AN	53	53	106
CrN	58	87	145
MeAN	67	99	176

A two dimensional cross section of the potential energy surfaces of acrylonitrile is given in Figure 6, with arrows indicating the pathway taken to reach the ground state. As can be seen from the figure, after excitation to S_1 or S_2 the C=C—C bending motion is inhibited by a potential energy barrier. The barrier to the C=C—C bend indicates that torsion occurs initially followed by bending. As noted earlier, the first and second excited states are nearly degenerate along the C=C torsion from the FC region. In the case of the methyl substituted analogs, a similar picture can be expected with a higher barrier to torsional motion on the second excited state.

D. Time-resolved photoelectron spectroscopy

The photoelectron spectra of AN, CrN, and MeAN are shown in Figures 7(a), 7(c), and 7(e). The time zero spectrum mainly exhibits a broad band that decays toward higher photoelectron kinetic energies and disappears around 4.5 eV (not shown). The ionization potential of AN is 10.92 eV[32,33] which is slightly more than the energy delivered by one pump (6.20 eV) and one probe photon (4.65 eV). Therefore, with the exception of the peak at 0 eV, ionization requires two probe photons which results in a total absorbed energy of 15.5 eV. More discussion on the photoelectron spectrum assignments can be found in the supplementary material.

The ionization potentials of MeAN and CrN have values of 10.34[32,34] and 10.23 eV,[32,35] respectively, both of which are below the [1 + 1′] threshold. This corresponds to the energy cutoffs at 0.51 and 0.62 eV in the photoelectron spectra, which agrees with the values found in our experiment (0.49 and 0.62 eV), although we note a minor peak at 0.61 eV in the MeAN spectrum. The signal at higher photoelectron kinetic energies (inset) originates from two-photon ionization. As in AN, we found that the amplitude of the photoelectron spectrum in the [1 + 2′] region decreases with increasing photoelectron kinetic energies.

Photoelectron spectra are commonly fit using a Levenberg-Marquardt 2D global fitting routine using the function

$$S(E,\Delta t) = \sum_{i=0}^{N_{\exp}} A_i(E) P_i(E,\Delta t) \otimes g(\Delta t). \quad (4)$$

Here, N_{exp} is the number of exponential functions used. $A_i(E)$ is the so-called *decay associated spectrum* which is associated with an exponential decay $P_i(E,\Delta t)$ of the form

$$P_i(E,\Delta t) = \exp(-\Delta t/\tau_i), \quad (5)$$

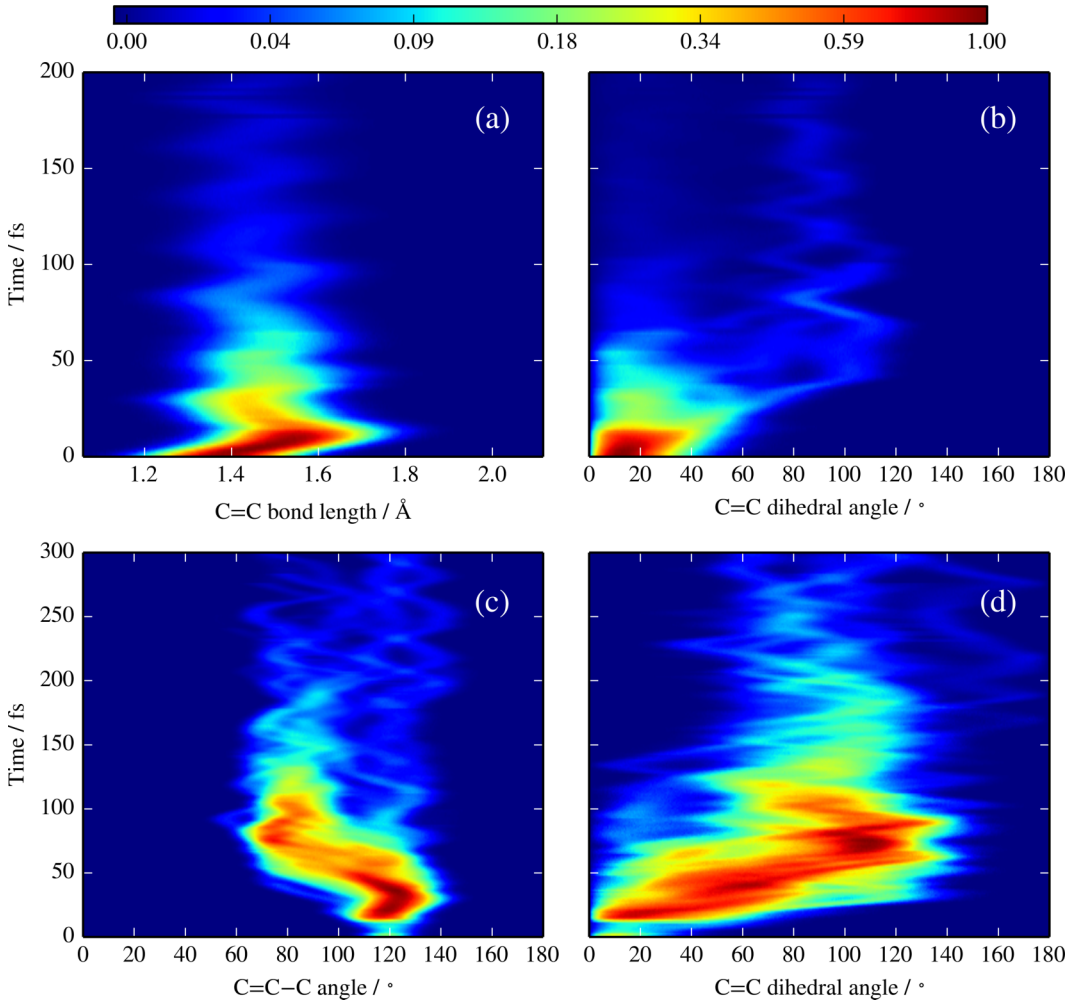

FIG. 5. Wavepacket density of AN along (a) the C=C bond length on S_2, (b) the C=C torsion on S_2, (c) the C=C—C bend on S_1, and (d) the C=C torsion on S_1. Most of the wavepacket on S_2 undergoes a single C=C stretch to reach S_1, followed by a C=C—C bend and C=C twist to reach S_0.

where $\Delta t = t - t_0$ is the pump-probe delay. The cross correlation $g(\Delta t)$ is determined independently (see Section II A).

This method of fitting is not able to describe all experimental data sets sufficiently well.[18,20,36] A temporal shift of the photoelectron band is observed which cannot be described satisfactorily with a set of exponentials, especially in the case where the Franck-Condon region exhibits a steep gradient on the excited state potential energy surface and the molecule undergoes large amplitude motion. This shift may lead to an increase in the ionization potential as the molecule deforms, yielding a "chirp" of the observed photoelectron kinetic energy signal. It has been previously demonstrated that one suitable way to describe this shift is by using time zero (t_0) of the experiment as a fitting parameter.[18,20,36] Assuming a monoexponential decay ($i = 1$), the spectrum is fit to the function

$$S(E,t) = A(E)\exp(-(t - t_0(E))/\tau_1) \otimes g(t - t_0). \quad (6)$$

The maximum shift therefore indicates the total electron kinetic energy signal modulation due to a dominant large amplitude vibrational mode. Note that the determined exponential decay time may be a varying function of the photoelectron kinetic energy as ionic channels may image the dynamics differently due to windowing effects.

The photoelectron spectra of AN, CrN, and MeAN could be fit with one exponential decay function, a non-zero offset that does not decay during the course of the experiment, and a shift in time zero for each energy channel. Time constants and maximum time zero shifts are summarized in Table II.

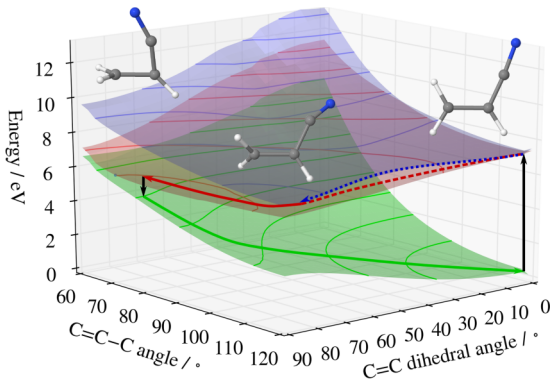

FIG. 6. 2D cross section of the acrylonitrile potential energy surfaces along the C=C torsion and C=C—C bend coordinates. Following excitation to S_2, the wavepacket follows a twist followed by a bend to reach S_0. Contour lines on the surfaces are given every 1 eV.

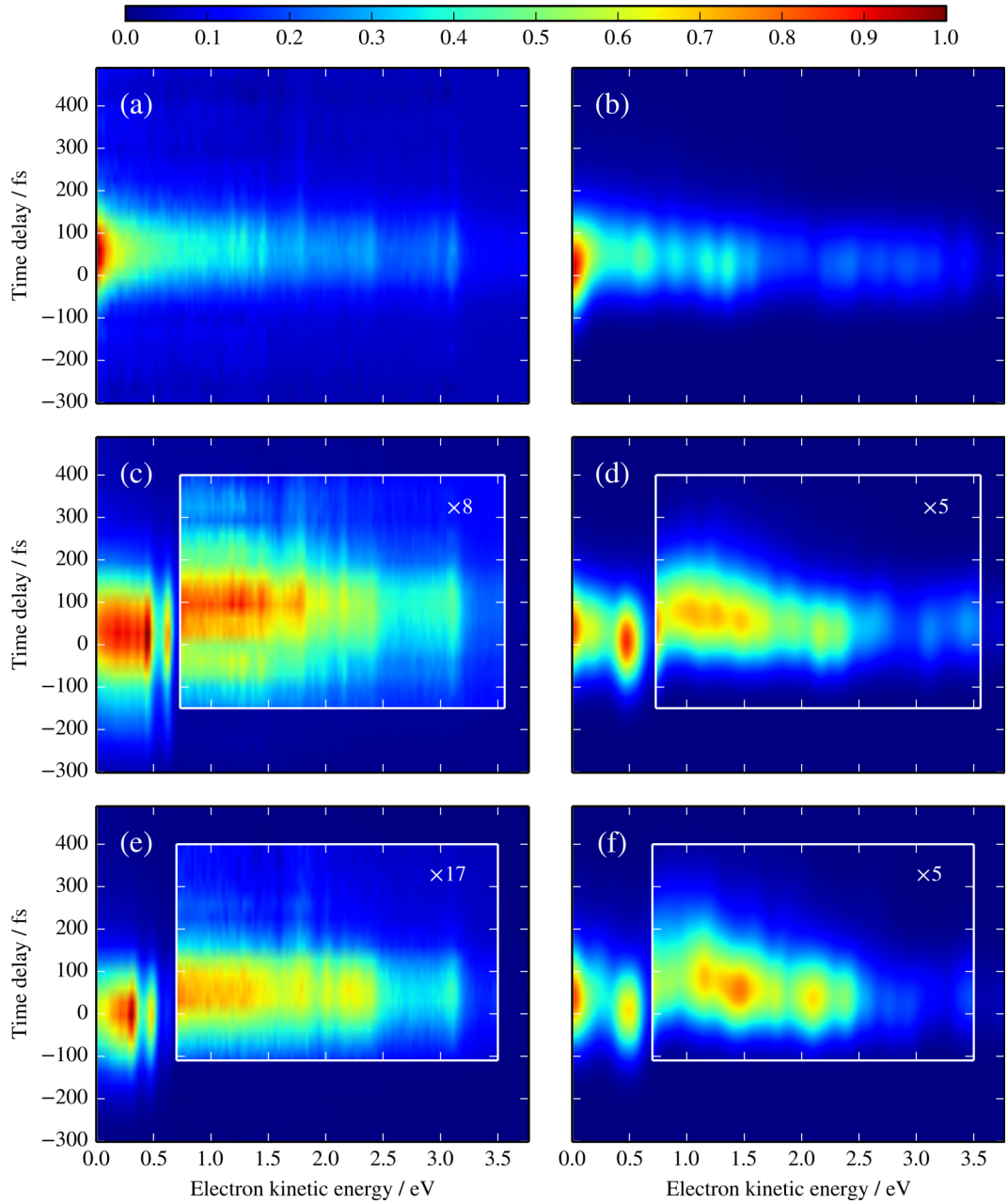

FIG. 7. ((a), (c), and (e)) Experimental and ((b), (d), and (f)) theoretical time-resolved photoelectron spectra of AN, CrN, and MeAN, respectively, using 200 nm pump and 267 nm probe wavelengths. Insets in CrN and MeAN spectra provide underlying data scaled by the given factor in order to show the 2-photon signals.

E. Simulation of the time-resolved photoelectron spectrum and comparison to the experimental data

In order to directly compare experimental and theoretical results, time-resolved photoelectron spectra were calculated from *ab initio* multiple spawning data as detailed in Section II B. The theoretical spectra are shown alongside experimental results in Figure 7. Other than signal from the 1-photon cutoff, data presented in the spectrum of AN are exclusively from two photon ionization as the ionization potential in the FC region is greater than that of [1 + 1′] ionization.[37] Spectra of CrN and MeAN contain both one and two photon signals, with insets showing the two photon regions of the spectra. The two photon ionization intensities in the calculated spectra were given a 1% weight relative to single photon results.

The energy correction of the dominant $S_1 \rightarrow D_0$ channel was found by comparing the experimental energy difference of 5.04 eV[10,37] to the calculated value of 2.56 eV. To account for errors in the *ab initio* ionization potentials, the difference

TABLE II. Maximum time zero shifts and global exponential decay time constants for fits of 2-photon experimental and theoretical TRPES spectra.

	Experimental		Theoretical	
Molecule	t_0^{max}/fs	τ_1/fs	t_0^{max}/fs	τ_1/fs
AN	37 ± 11	60 ± 10	55 ± 6	50 ± 2
CrN	44 ± 27	86 ± 11	59 ± 7	68 ± 3
MeAN	50 ± 28	97 ± 9	70 ± 9	81 ± 2

(2.49 eV) was subtracted from the computed photoelectron kinetic energies. However, in comparison to the experimental spectrum, the shift was changed to 1.96 eV for the 1-photon signal and 2.66 eV for the 2-photon signal to give the spectrum shown in Figure 7(b). For CrN and MeAN, spectra were adjusted to have approximately the same single photon energy cutoff as experimental results, yielding shifts of 1.87 for both CrN and MeAN in the 1-photon region and 2.06 and 2.19 eV, respectively, in the 2-photon region. The difference in energy shift is likely due to errors of calculated ionization energies for different transitions.

A detailed comparison of the experimental and simulated photoelectron spectra can be made by examining the fit parameters that are determined for both quantities using the model functions shown in Equations (4) and (6). Figure 8 provides a comparison of the time zero shifts as a function of electron kinetic energy for experiment and theory. The sum of the maximum shift of time zero and the corresponding time constant (t_0^{max} and τ_1, respectively) may be used as a lower bound of the excited state lifetime. The fit values of t_0^{max} for AN, CrN, and MeAN are 37 ± 11, 44 ± 27, and 50 ± 28 fs, and 60 ± 10, 86 ± 11, and 97 ± 9 fs for τ_1 as can be found in Table II. The combined maximum time zero shift plus the exponential decay accurately reproduce the total excited state lifetime of the molecules evinced in Table I. The error bars on the experimental quantities reflect the uncertainty in both the exponential fit as well as the data points in the photoelectron spectrum. The theoretical error bars were determined via repeated sampling of a subset of trajectories to quantify the uncertainty associated with employing a finite number of initial conditions.

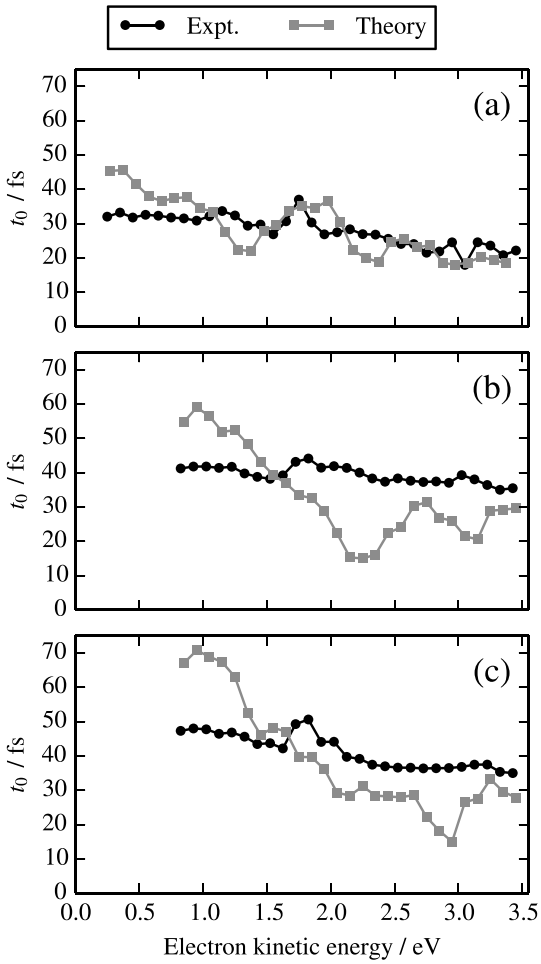

FIG. 8. Time zero shifts t_0 as a function of photoelectron kinetic energy for the 2-photon region of (a) AN, (b) CrN, and (c) MeAN.

These time constants can be compared to the experimental fitting in order to interpret the time constants observed in the experiments and to check the validity of the computations. The trend for the relaxation time of the molecules for the simulations is confirmed by the experiment both for the time zero shift as well as for the exponential decay time. In that sense, the experimental and simulated data of all three molecules agree in a satisfactory way. The total time for energy shifts plus exponential decays is 97, 130, and 147 fs, for AN, CrN, and MeAN, respectively, while the simulated spectra are slightly longer (105, 127, and 151 fs).

Time zero represents the time of an initial signal with a given electron kinetic energy. Thus, in each spectrum, the point $t_0 = 0$ occurs at the 1- and 2-photon energy cutoffs. The 1-photon cutoff can be seen as an energy localized peak in the spectra of CrN and MeAN at 0.49 and 0.62 eV, respectively. As the wavepacket evolves, its reduction in potential energy can be seen by a "chirp" towards lower electron kinetic energy at longer time delays (see Figure 8). The difference between the experimental and theoretical time zero shifts and exponential decay constants in Figure 8 occurs at energies near the maximum time zero shift. This suggests an overestimation of the change in potential energy during the low amplitude motion which causes the shift in t_0.

IV. DISCUSSION

The addition of a methyl group to AN influences the nonadiabatic dynamics by slowing the decay, as inferred from time constants for the decay of adiabatic populations and the TRPES signal. The excited state decay slowed from AN to CrN to MeAN. Considering the importance of torsional motion of the methylene (CH_2) group in AN in particular, it may be expected that methyl substitution of a methylene hydrogen should significantly affect the decay to S_0 by slowing rotation about the C=C bond. For this reason, intuition might suggest that substitution of one of the methylene hydrogens (yielding CrN) would have a more significant impact on the decay of the excited state population than replacement of a methine hydrogen (to form MeAN).

This analysis fails to account for the fact, however, that the requisite pyramidalization occurs almost exclusively at the 2-carbon. As discussed previously in studies of butadiene[31] and ethylene,[30] pyramidalization is accompanied by a sudden polarization across the unsaturated C=C bond. This polarization is engendered by the torsion about the internuclear axis which "decouples" the p-orbitals that form a π-bond. The presence of the electron donating cyano group bonded to C2 *ensures* that the negative charge develops almost exclusively at this site. Figure 9 clearly shows this effect by constructing a histogram of the partial (Mulliken) charges at

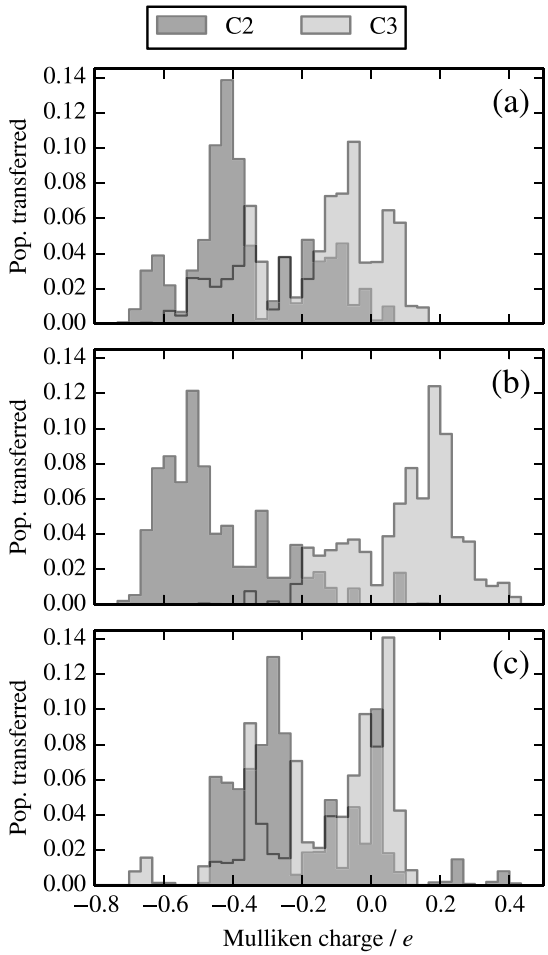

FIG. 9. Distribution of Mulliken point charges on S_1 at the Tw-C2P spawn points of (a) AN, (b) CrN, and (c) MeAN.

both the 2- and 3-carbons computed at each of the spawn geometries. As the figure evinces, the predilection for the molecules to pyramidalize at C2 is strongly correlated to the partial negative charge developed at this atomic site.

Furthermore, the dynamics simulations show that the longer lived excited state in MeAN is due to more than just a slowed pyramidalization vibration at the C2 site. As Figure 10 shows, appreciable wavepacket density is trapped on the S_1 excited state for multiple vibrational periods of the C=C—C angle bend and the methylene torsion mode. In contrast, over half of the AN population transfers to S_0 after a C=C—C bend in Figure 5. However, the fact that multiple passes through the coupling region are required to transfer amplitude to the ground state suggests that the region of the intersection seam accessed by the MeAN wavepacket is less efficient at mediating the nonadiabatic transition.

To elucidate this issue, we plot S_1 and S_0 potential contours along the C=C—C bending, C=C torsion, and H (CH_3) out-of-plane motion about the Tw-C2P MECIs, shown in Figure 11. The seam of intersection is plotted as a solid blue line and the point of MECI as a blue triangle. The spawn geometries are plotted as dots, the opacity of which indicate the amplitude of population transferred to S_0. To summarize, these plots show *where* population is transferred to the ground state and the relation of these points to the seam of intersection.

The results for AN and CrN (first two rows of Figure 11, respectively) show that the spawn points cluster *about* the MECI, with arguably a slight preference for larger out-of-plane angles than those displaying at the minimum energy crossings (26.6° and 33.6° for AN and CrN, respectively). In contrast, Figures 11(e) and 11(f) show that in the case of MeAN, the spawn points occur at uniformly larger pyramidalization angles than that of the MECI and thus at higher energies of the seam of intersection. This is likely due to the comparatively small CH_3 out-of-plane angle at the MECI for MeAN. Homoconjugation between the methyl C–H σ bond and the π orbitals on the C-backbone is a stabilizing influence as long as the CH_3 group remains in plane so that overlap can be maintained. For this reason, the corresponding pyramidalization angle at the S_1-S_0 MECI in MeAN is only 9.3° (compared to 26.6° and 33.6° for AN and

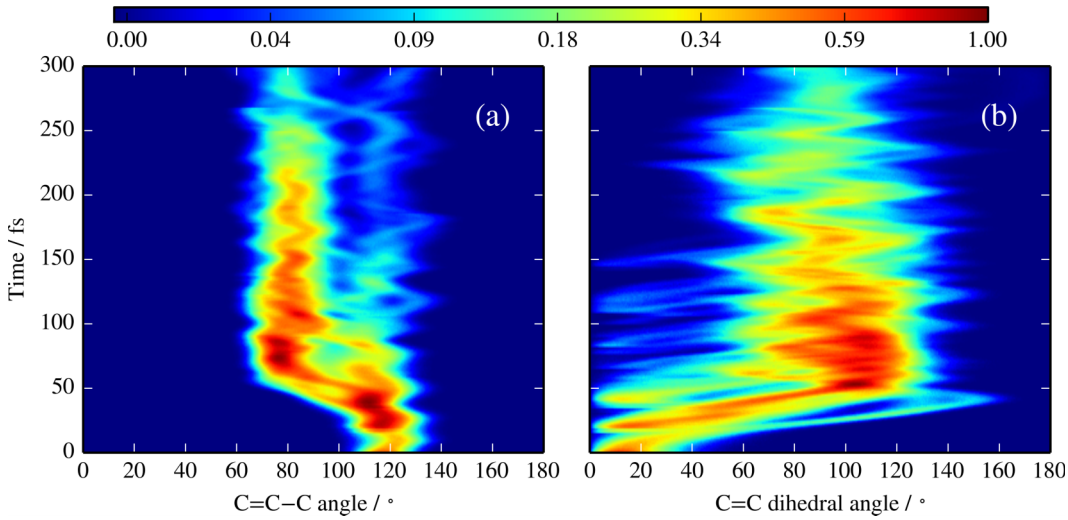

FIG. 10. MeAN wavepacket density projected onto S_1 along (a) the C=C torsion and (b) the C=C—C bend degrees of freedom. Unlike AN and CrN, the MeAN density takes multiple vibrations to fully transfer to S_0.

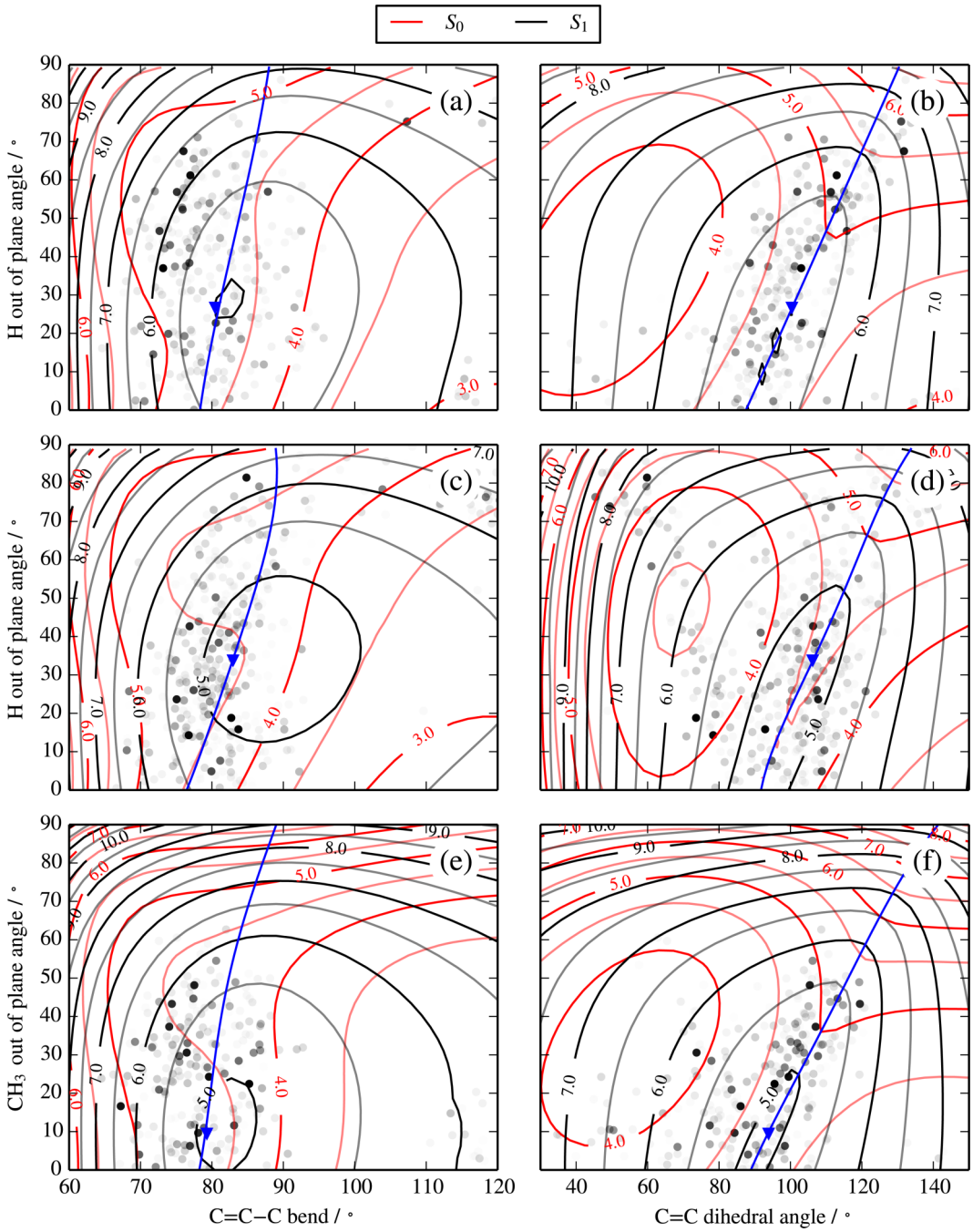

FIG. 11. S_1 and S_0 potential energy surfaces along ((a), (c), and (e)) C=C—C angle and H (CH_3) out-of-plane angle and ((b), (d), and (f)) C=C dihedral angle and H (CH_3) out-of-plane angle for AN, CrN, and MeAN, respectively. Blue triangles represent the Tw-C2P MECIs and blue lines are the paths of minimum energy difference between surfaces. Black dots are shown at AIMS spawn geometries with opacity representing the total population transferred.

CrN, respectively). The ensuing wavepacket dynamics are thus sampling higher energy regions of the intersection seam, with less symmetric intersection topologies (see the supplementary material), and thus lower nonadiabatic transition efficiencies.

V. CONCLUSIONS

In previous work,[15,16] we have examined how methyl substitution can be used to alter the frequency of particular vibrational modes, thereby influencing how an excited state wavepacket approaches a CI and thus the excited state lifetime. The premise in that work is that inertial substituents can be employed to direct wavepacket dynamics to some degree and engender some degree of "chemical control." In this work, the effect of methyl substitution was clearly observed in the measured (and simulated) excited state decay constants, significantly lengthening the excited state lifetime when placed at the medial carbon, as is the case for MeAN. From a purely dynamical perspective, the pyramidalization in the "twisted-pyramidalized" CIs would be predicted to occur at the *terminal* methylene carbon, given that the vibrational frequency for this mode (939 cm^{-1}) is significantly higher than at the medial carbon (672 cm^{-1}). However, it is the

capacity for electron donation of the cyano group which forces the partial negative charge (a key facet of pyramidalization) to develop at the medial carbon that drives the dynamics, not the inertial effects of the substituents. In other words, it is an electronic structure effect created by the cyano group that determines the relative rates of internal conversion and not the dynamical effect engendered by the increased inertia of the methyl groups. These results demonstrate that a general understanding of the dynamics at CIs will need to consider the interplay of these potentially competing effects.

SUPPLEMENTARY MATERIAL

See the supplementary material for molecular geometries, MR-FOCI/6-31G* and CASPT2/cc-pVTZ energies, CI analysis, and assignment of the AN photoelectron spectrum.

ACKNOWLEDGMENTS

R.M. and M.S. acknowledge financial support from the National Science and Engineering Research Council of Canada (NSERC). R.M. acknowledges the Government of Ontario for support in the form of an Ontario Graduate Scholarship. O.S. thanks the Wenner-Gren foundation for a research fellowship. R.F. acknowledges financial support by the Swedish Research Council (VR) and the Knut and Alice Wallenberg Foundation, Sweden. We would also like to thank Andrey Boguslavskiy for help with the uncertainty analysis.

[1]H. Okabe and V. H. Dibeler, J. Chem. Phys. **59**, 2430 (1973).
[2]G. A. West and M. J. Berry, J. Chem. Phys. **61**, 4700 (1974).
[3]J. B. Halpern, G. E. Miller, H. Okabe, and W. Nottingham, J. Photochem. Photobiol. A **42**, 63 (1987).
[4]A. Gandini and P. A. Hackett, Can. J. Chem. **56**, 2096 (1978).
[5]W.-N. Du, C. Luo, and Z.-S. Li, J. Chem. Phys. **129**, 174309 (2008).
[6]C. A. Bird and D. J. Donaldson, Chem. Phys. Lett. **249**, 40 (1996).
[7]C. Y. Oh, S. K. Shin, H. L. Kim, and C. R. Park, J. Phys. Chem. A **107**, 4333 (2003).
[8]P. A. Mullen and M. K. Orloff, Theor. Chim. Acta **23**, 278 (1971).
[9]F. Motte-Tollet, D. Messina, and M.-J. Hubin-Franskin, J. Chem. Phys. **103**, 90 (1995).
[10]S. Eden, P. Limão-Vieira, P. Kendall, N. J. Mason, S. V. Hoffmann, and S. M. Spyrou, Eur. Phys. J. D **26**, 201 (2003).
[11]V. Ilakovac, S. Carniato, J.-J. Gallet, E. Kukk, D. Horvatić, and A. Ilakovac, Phys. Rev. A **77**, 012516 (2008).
[12]V. Ilakovac, Y. Houari, S. Carniato, J.-J. Gallet, E. Kukk, and D. Horvatić, Phys. Rev. A **85**, 062521 (2012).
[13]K. Wang, V. McKoy, P. Hockett, and M. S. Schuurman, Phys. Rev. Lett. **112**, 113007 (2014).
[14]M. S. Schuurman, J. Giegerich, K. Pachner, D. Lang, B. Kiendl, R. J. MacDonell, A. Krueger, and I. Fischer, Chem. Eur. J. **21**, 14486 (2015).
[15]S. P. Neville, Y. Wang, A. E. Boguslavskiy, A. Stolow, and M. S. Schuurman, J. Chem. Phys. **144**, 014305 (2016).
[16]G. Wu, A. E. Boguslavskiy, O. Schalk, M. S. Schuurman, and A. Stolow, J. Chem. Phys. **135**, 164309 (2011).
[17]O. Schalk, A. E. Boguslavskiy, and A. Stolow, J. Phys. Chem. A **114**, 4058 (2010).
[18]T. J. A. Wolf, T. S. Kuhlman, O. Schalk, T. J. Martínez, K. B. Møller, A. Stolow, and A.-N. Unterreiner, Phys. Chem. Chem. Phys. **16**, 11770 (2014).
[19]A. M. D. Lee, J. D. Coe, S. Ullrich, M.-L. Ho, S.-J. Lee, B.-M. Cheng, M. Z. Zgierski, I.-C. Chen, T. J. Martínez, and A. Stolow, J. Phys. Chem. A **111**, 11948 (2007).
[20]O. Schalk, M. S. Schuurman, G. Wu, P. Lang, M. Mucke, R. Feifel, and A. Stolow, J. Phys. Chem. A **118**, 2279 (2014).
[21]J. H. D. Eland, O. Vieuxmaire, T. Kinugawa, P. Lablanquie, R. I. Hall, and F. Penent, Phys. Rev. Lett. **90**, 053003 (2003).
[22]T. Kłoda, A. Matsuda, H. O. Karlsson, M. Elshakre, P. Linusson, J. H. D. Eland, R. Feifel, and T. Hansson, Phys. Rev. A **82**, 033431 (2010).
[23]T. J. Martínez, M. Ben-Nun, and R. D. Levine, J. Phys. Chem. **100**, 7884 (1996).
[24]T. J. Martínez, M. Ben-Nun, and R. D. Levine, J. Phys. Chem. A **101**, 6389 (1997).
[25]M. Ben-Nun, J. Quenneville, and T. J. Martínez, J. Phys. Chem. A **104**, 5161 (2000).
[26]H. Lischka, R. Shepard, I. Shavitt, R. M. Pitzer, M. Dallos, T. Müller, P. G. Szalay, F. B. Brown, R. Ahlrichs, H. J. Böhm, A. Chang, D. C. Comeau, R. Gdanitz, H. Dachsel, C. Ehrhardt, M. Ernzerhof, P. Höchtl, S. Irle, G. Kedziora, T. Kovar, V. Parasuk, M. J. M. Pepper, P. Scharf, H. Schiffer, M. Schindler, M. Schüler, M. Seth, E. A. Stahlberg, J.-G. Zhao, S. Yabushita, Z. Zhang, M. Barbatti, S. Matsika, M. Schuurmann, D. R. Yarkony, S. R. Brozell, E. V. Beck, J.-P. Blaudeau, M. Ruckenbauer, B. Sellner, F. Plasser, and J. J. Szymczak, COLUMBUS, an *ab initio* electronic structure program, release 7.0, 2012.
[27]P. C. Hariharan and J. A. Pople, Theor. Chim. Acta **28**, 213 (1973).
[28]H. R. Hudock, B. G. Levine, A. L. Thompson, H. Satzger, D. Townsend, N. Gador, S. Ullrich, A. Stolow, and T. J. Martínez, J. Phys. Chem. A **111**, 8500 (2007).
[29]H. R. Hudock and T. J. Martínez, ChemPhysChem **9**, 2486 (2008).
[30]T. Mori, W. J. Glover, M. S. Schuurman, and T. J. Martínez, J. Phys. Chem. A **116**, 2808 (2012).
[31]B. G. Levine and T. J. Martínez, J. Phys. Chem. A **113**, 12815 (2009).
[32]K. N. Houk and L. L. Munchausen, J. Am. Chem. Soc. **98**, 937 (1976).
[33]J. Delwiche, M. Gochel-Dupuis, J. E. Collin, and J. Heinesch, J. Electron Spectrosc. Relat. Phenom. **66**, 65 (1993).
[34]G. D. Willett and T. Baer, J. Am. Chem. Soc. **102**, 6774 (1980).
[35]A. Chrostowska, T. X. M. Nguyen, A. Dargelos, S. Khayar, A. Graciaa, and J.-C. Guillemin, J. Phys. Chem. A **113**, 2387 (2009).
[36]O. Schalk, A. E. Boguslavskiy, A. Stolow, and M. S. Schuurman, J. Am. Chem. Soc. **133**, 16451 (2011).
[37]K. Ohno, S. Matsumoto, K. Imai, and Y. Harada, J. Phys. Chem. **88**, 206 (1984).